An Organism-Level Quantitative Flux Model of Mammalian Energy Metabolism

Bo Yuan [1], Karen E. Inouye [1,2], Gökhan S. Hotamışlıgil [1,2,3], Sheng Hui [1,2,4,*]

[1] Department of Molecular Metabolism, Harvard T. H. Chan School of Public Health, Boston, Massachusetts, USA.

[2] Sabri Ülker Center for Metabolic Research, Department of Molecular Metabolism, Harvard T.H. Chan School of Public Health, Boston, Massachusetts, USA.

[3] Broad Institute of Harvard and MIT, Cambridge, Massachusetts, USA.

[4] Lead Contact

* Correspondence: shui@hsph.harvard.edu (S.H.)

Keywords: isotope tracing, in vivo flux quantification, circulating nutrients, energy metabolism, obesity

Highlights

- A flux model of energy metabolism integrating ^{13}C labeling of metabolites and CO_2
- Circulating nutrients have characteristic partition between oxidation and storing
- Circulating nutrients' total cycling flux outweighs their total oxidation flux
- Cycling fluxes are extensively elevated in ob/ob but not diet-induced obese mice

24 **Graphical Abstract**

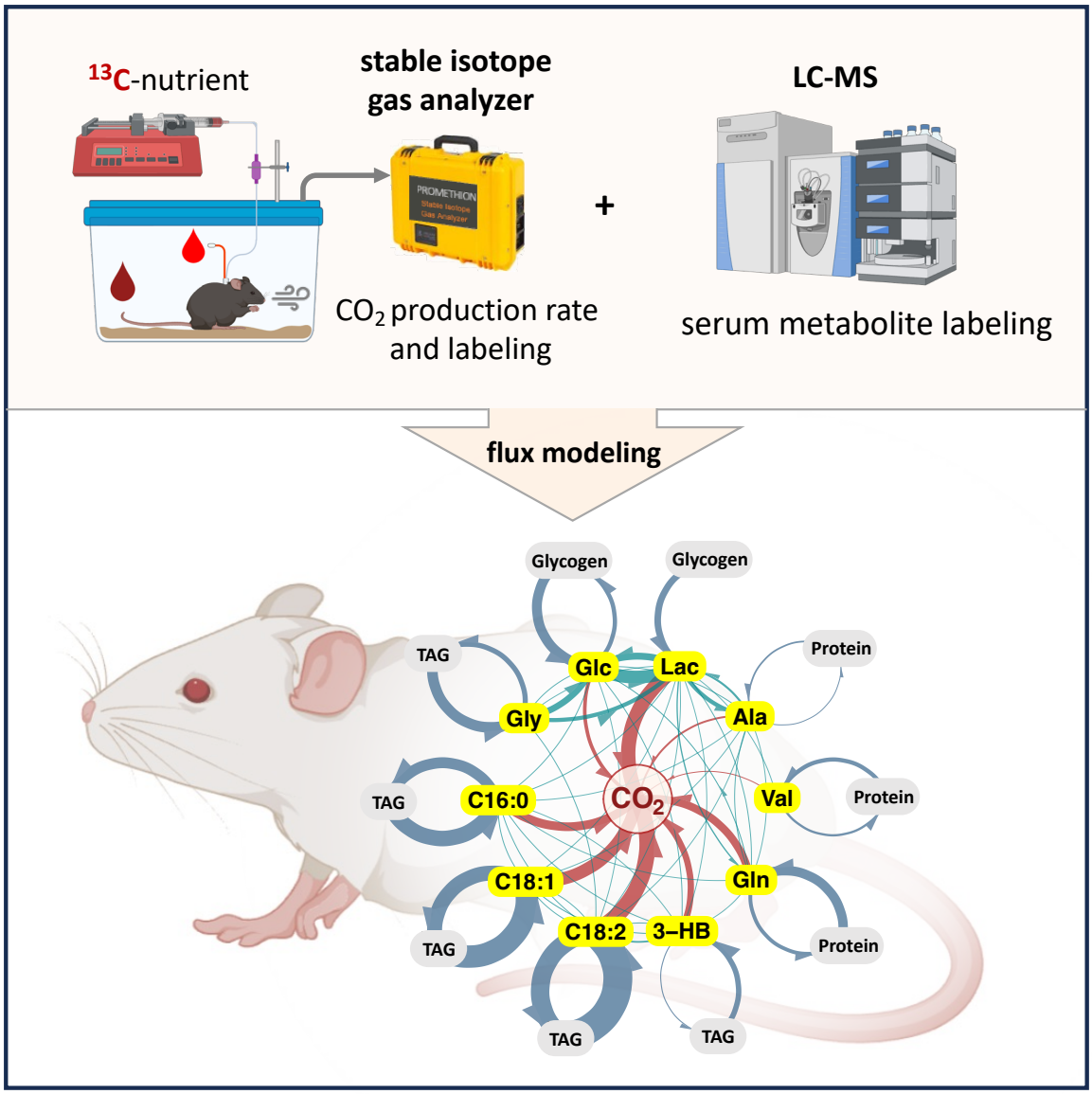

25

Summary

Mammalian tissues feed on nutrients in the blood circulation. At the organism-level, mammalian energy metabolism comprises of oxidation, interconverting, storing and releasing of circulating nutrients. Though much is known about the individual processes and nutrients, a holistic and quantitative model describing these processes for all major circulating nutrients is lacking. Here, by integrating isotope tracer infusion, mass spectrometry, and isotope gas analyzer measurement, we developed a framework to systematically quantify fluxes through these processes for 10 major circulating energy nutrients in mice, resulting in an organism-level quantitative flux model of energy metabolism. This model revealed in wildtype mice that circulating nutrients' metabolic cycling fluxes are more dominant than their oxidation fluxes, with distinct partition between cycling and oxidation flux for individual circulating nutrients. Applications of this framework in obese mouse models showed on a per animal basis extensive elevation of metabolic cycling fluxes in ob/ob mice, but not in diet-induced obese mice. Thus, our framework describes quantitatively the functioning of energy metabolism at the organism-level, valuable for revealing new features of energy metabolism in physiological and disease conditions.

INTRODUCTION

While our body is ultimately powered by nutrients in the food we eat, our tissues consume nutrients from the blood circulation for their energy needs, mostly by oxidizing them into CO_2. The circulating nutrients are supplied from digestion of food or breakdown of tissue nutrient storages such as glycogen and triacylglycerol (TAG). Instead of following the simple one-way process of release from storage to oxidation by tissues, however, a circulating nutrient can be simultaneously recycled back to its tissue storages, thus forming metabolic cycles (**Figure 1A**). For example, circulating glucose can be released from and resynthesized into tissue glycogen at the same time (Shipley et al., 1967, 1970). Another well-known example is the triacylglycerol-fatty acid cycle, which involves the simultaneous release of non-esterified fatty acid (NEFA) from tissue triacylglycerol (TAG) into circulation and resynthesis of tissue TAG from circulating NEFA (Nye et al., 2008; Reshef et al., 2003). In addition to the metabolic fates of oxidation and resynthesis into tissue storage, circulating nutrients also interconvert with each other, forming additional metabolic cycles (**Figure 1A)** (Hui et al., 2020). One prominent example is the Cori cycle, where circulating glucose is converted into circulating lactate, which is then converted back into circulating glucose through gluconeogenesis. Thus, circulating nutrients are involved in a complex network of fluxes, including those in oxidation, inter-nutrient metabolic cycling, and nutrient-storage metabolic cycling. Despite extensive knowledge of some well-known examples, a holistic and quantitative view of these fluxes encompassing all major circulating nutrients is lacking, preventing a global view of how energy metabolism is functioning in health and diseases such as obesity.

Here, we integrated isotope tracer infusion, mass spectrometry, and isotope gas analyzer measurement, and developed a fluxomics framework to calculate the oxidation, storing, inter-converting, and releasing fluxes for 10 major circulating nutrients in mice (**Figure S1**). The resulting quantitative flux model at the organism-level revealed many surprising features of mammalian energy metabolism. Of note, metabolic cycling flux is numerically more prominent than oxidation for circulating nutrients, despite the already enormous oxidative flux. To unravel the global changes of energy metabolism in obesity, we applied this framework on obesity models. Among our findings, compared with lean mice and on a per animal basis, the metabolic

71 cycling fluxes of carbohydrate and fat nutrients were elevated by about 2-fold in the leptin-
72 deficient obese mice while they remained largely the same in diet-induced obese mice. Overall,
73 our work provides a framework for building an organism-level flux model of energy metabolism,
74 a useful tool for metabolic research.
75
76 **RESULTS**
77 **Quantifying the Fraction of Oxidation for a Circulating Nutrient**
78 In general, the carbon atoms in a circulating nutrient either leave the body as the oxidation
79 product CO_2 or are recycled back into storages in the body (**Figure 1A**). To quantify these
80 oxidation fluxes and storing fluxes of circulating nutrients, we first aimed to determine what
81 fraction of a circulating nutrient is oxidized into CO_2, or its fraction of oxidation (f_{ox}). For this,
82 using circulating glucose as an example, we intravenously administered a small amount of ^{13}C-
83 uniformly labeled glucose as a single bolus into modestly fasted mice, and monitored the $^{13}CO_2$
84 production using a metabolic cage equipped with a $^{13}CO_2$ analyzer (**Figure 1B**). The production
85 flux of $^{13}CO_2$ peaked at around 30 min, significantly dropped in another 2 hours, and tailed to
86 approach background level within a total of 6 hours (**Figure 1B;** see calculation of $^{13}CO_2$ flux in
87 **Supplementary Note 1**). Integration of the $^{13}CO_2$ production kinetic curve over the 6 hours gives
88 the total $^{13}CO_2$ production from the tracer administered. The recovery was then calculated as the
89 ratio between the total production of $^{13}CO_2$ (μmol) and the administered tracer dose (μmol ^{13}C
90 atoms). Glucose recovery was thus determined to be 0.75. This suggests that 25% of circulating
91 glucose atoms were destined to storage pools, such as triglycerides, proteins, glycogen, and other
92 macromolecules. To verify this number, we intravenously injected the radioactive tracer ^{14}C-
93 glucose into mouse, and measured the remaining radioactivity in the carcass 6 hours after
94 administration. The carcass was digested into a solution, and the radioactivity was measured
95 using a scintillation counter. We detected 26% of the administered dose in the carcass (**Figure**
96 **1C**), consistent with our $^{13}CO_2$ measurement and a previous result (Tolbert et al., 1956).
97 To further confirm the glucose recovery result, instead of a bolus injection of ^{13}C-glucose,
98 we infused ^{13}C-glucose into the mouse systemic circulation via a pre-implanted jugular vein
99 catheter. Compared to the bolus injection, the constant infusion at a low rate reduces the

amount of exogenous nutrient per minute administered to the animal and thus minimizes potential perturbation to metabolism . Here the recovery is the ratio of $^{13}CO_2$ production rate (µmol/min) at steady state to the ^{13}C-infusion rate (µmol ^{13}C atoms/min). With this experiment, we measured glucose recovery to be 0.73 (**Figure 1D**), in close agreement with that measured with the bolus administration. We thus combined results from both methods and took the average as the recovery of glucose.

To obtain the f_{ox} value for glucose, we next took in account the fact that a portion of the $^{13}CO_2$ generated from oxidation of ^{13}C-glucose can undergo carboxylation and get incorporated into metabolite pools (such as urea and oxaloacetic acid) which are not recovered in the exhalation (Elia et al., 1992). For this, we intravenously infused ^{13}C-labeled bicarbonate, and determined a recovery of 90% for bicarbonate, indicating that 90% of produced CO_2 from substrate oxidation actually leaves the body as exhaled CO_2. We thus took the ratio of glucose recovery to bicarbonate recovery as the glucose f_{ox}, and obtained a value of 0.81 (**Figure 1E**). This value reflects that ~80% of circulating glucose is oxidized, and ~20% is recycled back to storage pools independent of the CO_2 carboxylation pathway.

Distinct f_{ox} Values for Different Circulating Nutrients

In addition to glucose, we went on to quantify the f_{ox} for 12 other circulating nutrients (**Figures 1E**, **S2A-D**). For most circulating nutrients investigated, the f_{ox} by both bolus injection and infusion methods are generally consistent (**Figure S2C**), and we pooled the data from both methods. Glycerol, however, was 30% more oxidized when administered as a bolus than by infusion, suggesting significant perturbation to glycerol metabolism by the bolus administration. Given the negligible perturbation by infusion, we used infusion-based f_{ox} for glycerol for further analyses.

Among all 13 circulating nutrients, lactate had the highest f_{ox} of around 100%, significantly higher than glucose f_{ox} of 81% (**Figure 1E**). This result further substantiates circulating lactate's role as an energy source for tissues (Hui et al., 2017). The ketone body 3-hydroxybutyrate and acetate also have high f_{ox} of 81% and 86%, respectively, indicating their main use as energy sources in the body. Non-esterified fatty acids (NEFA) occupy the lower end of the f_{ox} spectrum.

129 Palmitate (C16:O), oleate (C18:1), and linoleate (C18:2), the most abundant NEFAs in circulation,
130 have f_{ox} values of around 45%, suggesting prominent fluxes from circulating NEFAs back to tissue
131 triglycerides (Reshef et al., 2003). The branched-chain amino acid (BCAA) valine has a f_{ox} of only
132 32%, similar to that of BCAA leucine (Tolbert et al., 1956). Together with f_{ox} of 24~26% for the
133 essential amino acids methionine and tryptophan, this result reveals that the majority of
134 proteolysis-released circulating amino acids are recycled back into proteins. In contrast,
135 circulating glutamine and alanine have high f_{ox} of 77% and 84%, respectively, indicating their
136 unique roles in energy metabolism among amino acids. Thus, f_{ox} of a circulating nutrient reveals
137 its main role in mammalian metabolism and is a fundamental property of circulating nutrients.
138 In the following flux analysis, we focused on 10 nutrients in **Figure 1E**, which were the top
139 9 circulatory nutrients (Hui et al., 2017) and valine. Albeit a small circulatory turnover flux, valine
140 was included as a reporter of protein metabolism. The other 9 nutrients are glucose, lactate,
141 glycerol, alanine, glutamine, 3-HB, C16:0, C18:1, and C18:2.
142
143 **Quantifying Oxidation and Storing Fluxes of Circulating Nutrients**
144 Based on the f_{ox} measurement, we next sought to quantify the fluxes associated with oxidation
145 and storing destinies of circulating nutrients. At the steady state of ^{13}C-tracer infusion, we
146 sampled the blood and measured the ^{13}C-labeling of the infused nutrient using mass
147 spectrometry (**Figure 2A**). The serum labeling of the infused nutrient (L) reflects the dilution of
148 the infusate (at a rate R) by the endogenous production flux of the nutrient, which is thus equal
149 to $R\frac{1-L}{L}$. Since f_{ox} and $1-f_{ox}$ are the fraction of the circulatory flux that is fated to oxidation
150 and storing, respectively (**Figure 2B**), the oxidation and storing fluxes of a circulating nutrient
151 (denoted as J_{OX} and J_S, respectively) can be calculated (see derivation in **Supplementary note 2**)
152 as

$$J_{OX} = R\frac{1-L}{L}f_{ox} \tag{1}$$

$$J_S = R\frac{1-L}{L}(1-f_{ox}) \tag{2}$$

153 The absolute flux values reveal quantitatively the magnitude of each nutrient as an oxidation
154 substrate or storage precursor (**Figure 2C**). For example, though linoleic acid has lower f_{ox} than

155 glucose (**Figure 1E**), it has higher oxidation flux. Valine has the largest storing fraction ($1 - f_{ox}$),
156 but the associated storing flux is among the smallest.
157
158 **Quantifying *Direct* Oxidation and Storing Fluxes of Circulating Nutrients**
159 The oxidation flux for a circulating nutrient quantified above describes the nutrient's ultimate
160 disposal into CO_2. It includes both direct and indirect oxidation fluxes of the nutrient. The indirect
161 oxidation refers to the process that a circulating nutrient is first converted into other circulating
162 nutrients before being oxidized. For example, an important indirect oxidation route for
163 circulating glucose is via circulating lactate. In like manner, the storing flux also comprises both
164 the direct and indirect ways. To gain further insights on the sources and sinks of circulating
165 nutrients, we next sought to quantify the *direct* fate of a circulating nutrient to oxidation and
166 storage.
167 We denote the direct oxidation flux from a circulating nutrient i as O_i, which we aim to
168 calculate. Now consider the steady state of a nonperturbative infusion of a ^{13}C-labeled nutrient,
169 e.g., ^{13}C-glucose. The $^{13}CO_2$ production flux from the animal is given by Rf_{ox}, where R is the
170 infusion rate and f_{ox} is the glucose fraction of oxidation. As the $^{13}CO_2$ production is also equal to
171 the sum of labeled direct oxidation fluxes from all circulating nutrients, we have

$$\sum O_i^t L_i = Rf_{ox} \tag{3}$$

172 where O_i^t is the direct oxidation flux (including both ^{13}C and ^{12}C) of nutrient i, and L_i the labeled
173 fraction of the nutrient (illustrated in **Figure 3A**). As the endogenous unlabeled oxidation flux O_i
174 accounts for $1 - L_i$ fraction of O_i^t, or $O_i = O_i^t(1 - L_i)$, plugging it into the above equation gives
175 the expression with the endogenous oxidation flux O_i as the only unknown

$$\sum \frac{L_i}{1 - L_i} O_i = Rf_{ox} \tag{4}$$

176 This equation holds under the infusion of each different ^{13}C-labeled nutrient. As such, the infusion
177 of 10 different ^{13}C-nutrients unveils the inter-labeling pattern among these nutrients (**Figures 3B**
178 and **S3A**), and allows the construction of a linear system of 10 equations of

$$\boldsymbol{A} \cdot \begin{bmatrix} O_1 \\ O_2 \\ \vdots \\ O_{10} \end{bmatrix} = \begin{bmatrix} R_1 f_{ox_1} \\ R_2 f_{ox_2} \\ \vdots \\ R_{10} f_{ox_{10}} \end{bmatrix} \quad (5)$$

179 where $\boldsymbol{A}$ is a 10×10 matrix, with $L_i^j/(1-L_i^j)$ in the jth row and i^{th} column and L_i^j representing
180 the labeling of ith circulating nutrient under the infusion of the jth tracer. Solving these linear
181 equations yields the direct oxidation fluxes O_i of the circulating nutrients (**Figure 3C**). The direct
182 storing fluxes S_i can be calculated in the same manner (**Figure 3C**; see more details in derivation
183 in **Suppl. Note 3**).
184
185 **Direct Contribution of Circulating Nutrients to Total Energy Expenditure**
186 The direct oxidation fluxes form an organism-level view of burning circulating nutrients for
187 energy (**Figure 3**). Compared with the total CO_2 exhaled by the animal measured directly using a
188 metabolic cage, the 10 nutrients alone accounted for about 80% of the total CO_2 production,
189 confirming that these nutrients represent the top circulating nutrients. Glucose, while being the
190 most famous energy nutrient, has rather minimal direct oxidation flux, accounting for only
191 marginal fraction of total energy expenditure (TEE) (**Figure 3C**). Instead, circulating lactate,
192 mostly derived from glucose, is the dominant carbohydrate that directly fuels oxidation (Hui et
193 al., 2017), responsible for about 20% of TEE. Glutamine, as the single most important amino acid
194 fuel, contributes to 7% of TEE, while alanine and valine contribute 1.5% and 0.7%, respectively.
195 As the oxidative disposal of essential amino acid reflects the use of proteins for energy
196 expenditure, based on the content of valine (5%) in muscle proteins (Gorissen and Phillips, 2018),
197 the direct oxidation of protein-originated amino acids can be estimated to provide approximately
198 14% of TEE (Fearon et al., 1988; Matthews et al., 1980). The ketone body 3-HB contributes to 5%
199 of TEE. Due to the rapid equilibrium between 3-HB and acetoacetate, this quantity reflects the
200 contribution of the total ketone bodies (Keller et al., 1981). The three NEFA species, palmitate,
201 oleate, and linoleate, are among the most prominent fuels, contributing to 8%, 15% and 22% of
202 TEE, respectively, or 45% in sum. As these top 3 NEFAs account for about 75% of total NEFA in
203 circulation (**Figure S3C**), approximately 60% of TEE is supported by the total NEFA in circulation.
204 Glycerol is uniquely the only nutrient that is not directly engaged in oxidation (Hui et al., 2020).

All nutrients considered together, using both direct measurement and empirical extrapolation, close to 100% of TEE can be quantitatively accounted for (**Figure 3D**, showing the direct TEE contribution from carbohydrate nutrients (glucose, lactate, and glycerol), NEFAs, protein, and ketone bodies).

Recycling to Storage Is a Highly Prominent Fate of Circulating Nutrients

The direct storing fluxes revealed the composition of nutrients for resynthesizing fuel storages. The total NEFAs present a dominating 60% of the total storing flux (**Figure 3D**). Amino acids also have prominent storing fluxes. Using valine as a representative of protein-originated amino acids, the total amino acids storing flux accounts for 30% of the total storing flux. Carbohydrates have a minor part (6%) in the total storing flux, with lactate having zero direct storing flux. This again highlights lactate's role as a fuel metabolite. Most strikingly, all circulating nutrients considered together, the total storing flux is 23% higher than that of oxidation (**Figure 3D**), vividly demonstrating the enormity of futile cycling fluxes of circulating nutrients.

Quantifying Inter-converting Fluxes between Circulating Nutrients and their Releasing Fluxes from Storages

We have so far focused on oxidation and storing as destinies for circulating nutrients. The storages however also serve as sources for circulating nutrients. To work toward a full view of metabolism of circulating nutrients, here we attempted to quantify the production fluxes of the circulating nutrients from the storage pools. In the same calculation, we also obtained the interconverting fluxes between circulating nutrients, which was a main result in our previous work (Hui, et al. 2020).

To illustrate the calculation, we use glucose as an example and quantify its production fluxes, including the storage releasing flux F_S, i.e., glycogenolysis, and the gluconeogenic flux F_i from circulating nutrient i (**Figure 4A**). Now consider the steady state during a nonperturbative ^{13}C-glucose infusion with an infusion rate R. The total incoming flux (F_{total}) to the glucose pool, which at steady state is equal to the total outgoing flux of glucose, is given by

$$F_{total} = R + \sum_i F_i^t + F_S \quad (6)$$

233 where $F_i^t = \frac{F_i}{1-L_i}$ with L_i the labeling of nutrient i. Note that F_i^t is the total flux from nutrient i
234 to glucose including both endogenous unlabeled flux F_i and labeled flux $F_i^t L_i$. The mass balance
235 of the labeled glucose pool (with the labeling denoted as L_{glc}) requires

$$\sum_i F_i^t L_i + R = F_{total} L_{glc} \quad (7)$$

236 where the left-hand-side is the incoming labeled glucose flux and the right-hand-side the
237 outgoing labeled glucose flux. Eq. (5) and the expression for F_i^t can be plugged into Eq. (6) to
238 form an equation with F_i's and F_S as the only unknowns (Methods). Such an equation holds
239 under the infusion of other ^{13}C-nutrients, but with $R = 0$. With infusions of ^{13}C glucose and 9
240 other ^{13}C-labeled circulating nutrients, a linear system of 10 equations can be then constructed
241 for the 10 unknowns including the 9 F_i's and F_S, in like manner as Eq. (4). Solving the equations
242 yielded the storage releasing flux, and the conversion fluxes from the 9 circulating nutrients, to
243 produce circulating glucose. In similar fashion, the releasing fluxes and inter-converting fluxes
244 can be calculated for other circulating nutrients using the same computational framework. More
245 derivation details can be found in **Suppl. Note 4**.
246

247 **Sources of Circulating Nutrients**

248 The storage releasing flux and inter-converting flux results calculated above provide a
249 quantitative view of the direct sources for each of the 10 circulating nutrients (**Figure 4B**). Two
250 types of circulating nutrients can be seen, nutrients directly sourced from the storages, and those
251 derived from both storages and other circulating nutrients. NEFA and glycerol are almost
252 exclusively released from the TAG store, and valine and glutamine from the protein store. In
253 contrast, glucose, lactate, alanine, and 3-HB are additionally sourced from other circulating
254 nutrients. For circulating glucose, about 40% is released from glycogen, while the remaining
255 majority is produced by gluconeogenesis, primarily from lactate and glycerol (each about 25%).
256 For circulating lactate, about 20% is released from glycogen, in line with that measured by pulse-
257 chase tracing of glycogen (TeSlaa et al., 2021), while the remaining mostly comes from glucose

258 (60%) and glycerol (10%). As glycerol is derived from TAG, this collectively shows that glycogen
259 and TAG but not protein are the major ultimate sources of circulating glucose (Wang et al., 2020).
260 We further quantified such ultimate contribution fraction from various storages to circulating
261 nutrients (**Figure S4A**, see derivation in **Suppl. Note 5**). Interestingly, while amino acids are
262 typically released from the protein as the principal source, alanine has its carbon origin roughly
263 evenly from protein, glycogen, and TAG.
264
265 **Sinks for Circulating Nutrients**
266 Together with the direct oxidation and storing fluxes calculated earlier (**Figure 3C**), the inter-
267 conversion fluxes of circulating nutrients constitute the direct sinks of circulating nutrients
268 (**Figure 4C**). This integrated view offers interesting insights. For example, though glutamine and
269 alanine, are known to be gluconeogenic, their direct conversion to lactate is more predominant
270 than to glucose. In addition, these amino acids are directly oxidized with higher fluxes than
271 otherwise relying on the lactate-genic pathway for energy supply.
272
273 **A Flux Model Incorporating All Quantified Fluxes for Circulating Nutrients**
274 A further inclusive combination of the production and consumption fluxes resulted in a
275 comprehensive metabolic flux model of circulating nutrients (**Figure 4D**). In addition to the
276 prominent oxidative fluxes for energy generation, this model vividly highlights two types of
277 cycling of the circulating nutrients. One type involves the cycling between the circulating
278 nutrients and the storages, and a second cycling exists between the circulating nutrients. These
279 cycles render a picture of vibrant carbon exchanges among nutrients in circulation and tissues.
280 Many of the futile cycles proceed at the cost of ATP. We estimated ATP wasted in the Cori cycle,
281 TAG-NEFA cycling, and protein turnover, the top three cycles with the highest carbon flux
282 (Methods). Together, these cycles wasted remarkably around 10% of the total ATP generated
283 (**Figure S4B**).
284
285 **Fluxes Are Generally Unperturbed in Diet-Induced Obese Mice**

286 To further demonstrate the utility of the systems-level flux modeling, we applied the framework
287 to two obese mouse models, high fat diet-induced obese mice (HFD), and leptin-deficient ob/ob
288 mice (**Figures 5-6, S5**). Unexpectedly, despite being 60% heavier than the wild type control mice
289 on chow diet, the HFD mice showed generally moderate changes in f_{ox} and fluxes (**Figures 5A-**
290 **D**). The most striking change is the significantly increased production of glycerol from circulating
291 glucose, i.e., the recently discovered glycerol shunt pathway (**Figures 5B**; **S6, S7A**)(Mugabo et al.,
292 2016; Possik et al., 2023). This pathway is quantitatively negligible in WT; while it was elevated
293 by 2-fold in ob/ob mice, it was more impressively activated by 4.5 fold in the HFD group.
294
295 **Extensive Elevation of Metabolic Cycling in ob/ob Mice**
296 In contrast to the HFD mice, ob/ob mice showed major changes in energy metabolism. While f_{ox}
297 was moderately decreased for many nutrients, it was most prominently decreased by 2-fold in
298 circulating NEFAs (**Figures 5A**). This was accompanied by a 2-fold increase on average in the
299 circulatory turnover flux (equal to total consumption flux and total production flux) of NEFAs,
300 resulting in unchanged oxidation flux, but a 2.3-fold elevation in the circulating NEFA recycling
301 flux (**Figures 5B-D**). Intracellular reesterification nonetheless remained unchanged (**Figure S7B**).
302 The circulatory fluxes of both glucose and lactate were also increased by around 2-fold, with
303 production from different sources roughly proportionally scaled up. This led to a 2.3-fold increase
304 in the oxidation of the carbohydrate nutrients, and drove an increase in total energy expenditure
305 in ob/ob mice. This was accompanied with over 2-fold increase in the fluxes of glucose recycling
306 to storage and Cori cycle. Interestingly, as gauged by the essential amino acid valine, the global
307 protein oxidation and futile recycling remains unchanged. All nutrients considered, the futile
308 storing flux is 60% higher than their oxidation flux. The total ATP wasted in the top 3 futile cycles,
309 TAG-NEFA extracellular recycling, Cori cycle and protein turnover, was 34% higher in ob/ob mice
310 than the chow-fed control mice (**Figure S7C**).
311
312 **DISCUSSION**
313 The present flux framework is a major advancement over our previous work (Hui et al., 2020),
314 where we systematically quantified the inter-converting fluxes between circulating nutrients

using isotope labeling data of serum metabolites. Here, by incorporating additional measurements of production rate and isotope labeling of exhaled CO_2, our framework further outputs the oxidation, storing and releasing fluxes of circulating nutrients. Together with the inter-converting fluxes, these fluxes form a full account of sources and sinks for circulating nutrients at the organism level, resulting in a coherent flux model of energy metabolism. Analogous to a map showing traffic along major highways in a city, our flux model captures the top fluxes in an animal body, providing an overview of energy metabolism landscape for the animal. Such a flux model for a disease state reveals unbiasedly the major alterations in energy metabolism for that disease, setting the stage for further investigations.

Our flux model revealed extensive metabolic cycling in the fasted state, with higher total flux than total oxidation flux. During fasting, the animal body is in a net catabolic state, with nutrient storages such as glycogen, TAG, and proteins being actively broken down to replenish circulating nutrients for oxidation into CO_2. Yet, recycling back into the storage pools is a quantitatively more significant fate for circulating nutrients. What is the function of the extensive cycling? One hypothesis is that it is to produce heat, to maintain or elevate body temperature (Brownstein et al., 2022; Oeckl et al., 2022; She et al., 2007; Wolfe et al., 1987). We estimated substantial energy used by these futile cycles, about 10% total ATP generated. Another probable hypothesis is that metabolic cycling is to increase the sensitivity of metabolic regulation by enhancing the response magnitude for changes in the stimulus (e.g., substrate concentration)(Newsholme, 1978). We further revealed distinct partition between oxidation and cycling fluxes for different circulating nutrients, e.g., about 80% of circulating glucose is burned, while it is only ~40% for a fatty acid, and ~30% for an essential amino acid. The larger extent of metabolic cycling in fatty acids and amino acids may thus reflect their relatively less hormonal control than glucose. These and other hypotheses regarding the underlying principles of the presence of extensive cycling flux and of distinct f_{ox} values across nutrients deserve further investigations.

Our comprehensive flux results allows for comparison of fluxes between processes and can expose flux mismatches and thus knowledge gaps. This way, we identified an important gap in our understanding of the TAG-NEFA cycle, specifically regarding the sources of glycerol

344 backbone for resynthesis of TAG. The flux through the TAG-NEFA cycle constitutes the major
345 fraction of metabolic cycling, indicating active re-esterification of circulating NEFAs. As adipose
346 tissues are the predominant site of TAG, much of this re-esterification must happen in adipose
347 tissues. Glucose is classically viewed as the main source for glycerol backbone in TAG synthesis
348 in adipose tissues. However, even if all the glucose storing flux is diverted to adipose tissues for
349 producing glycerol backbone, it would be far from sufficient to meet the demand (Figure S5G).
350 Though lactate has been proposed as a supply of the glycerol carbons in the adipose tissue via
351 the glyceroneogenesis pathway (Hanson et al., 2006), our data shows that circulating lactate has
352 negligible direct flux fated to storages. Instead, our quantification points to another possibility:
353 TAG resynthesis is sustained by recycling glycerol from circulation back to adipose tissue, and the
354 glycerol's storing flux quantitatively fulfills most of the needed glycerol backbone for TAG-
355 resynthesis (Figure S6). However, as adipose tissue lacks glycerol kinase, it may be postulated
356 that glycerol enters the adipose tissue TAG in the form of diacylglycerols or monoacylglycerols,
357 which are in turn derived from liver-made VLDL-TAG. To elaborate, in this pathway, NEFA and
358 glycerol are first packed into VLDL-TAG in the liver, and transported to the adipose tissue, where
359 lipoprotein lipase (LPL) is highly expressed (Coppack et al., 1999; Kleberg et al., 2014). The LPL
360 hydrolyzes TAG into fatty acids and di- and monoacylglycerols, which can be efficiently extracted
361 into the adipose tissue (Scow and Blanchette-Mackie, 1991). The acylglycerols are directly
362 synthesized into TAG sequentially by mono- and di-acylglycerol acyltransferases in the adipose
363 tissue (Liss et al., 2018; Shi and Cheng, 2009). Further investigations are needed to test this
364 hypothesis.

365 Our flux results for the two obesity models demonstrated strikingly distinct energy
366 metabolism between them. Energy metabolic fluxes were mostly maintained in the HFD mice
367 while there was extensive elevation of cycling fluxes in the ob/ob mice. Though we cannot rule
368 out body weight as a contributing factor (45 g HFD mice versus 60 g ob/ob mice), as the control
369 mice (30g) were much smaller, the flux differences more likely reflect their intrinsic distinctions.
370 It is possible that the HFD mice resemble the "healthy obesity" group in human population, who
371 are metabolically healthy despite being obese. On the other hand, the ob/ob mice lie in a totally
372 different part of the energy metabolism space, possibly mirroring their departure from the state

373 of metabolic health. Thus, instead of the commonplace view that ob/ob mice are an "artificial"
374 obesity model, HFD mice and ob/ob mice may model two states along the progression of obesity.
375 Further flux studies using weight-matched groups will test this hypothesis.
376 The elevated glucose production and consumption fluxes in ob/ob mice inform on the
377 cause of hyperglycemia. In general, an increase of a metabolite pool could result from either a
378 blockage in the consumption reactions or an elevation in the production reactions. As production
379 and consumption balance each other in the new steady state, the flux through the pool can be
380 either reduced (in the consumption blockage case) or increased (in the production elevation case)
381 compared to the unperturbed state. By this argument, the increased flux through the glucose
382 pool in the ob/ob mice indicates elevated glucose production as the cause of hyperglycemia,
383 implicating liver insulin resistance instead of muscle insulin resistance as the driver of
384 hyperglycemia.
385
386 **Limitation**
387 The identities of nutrient storages were not explicitly studied in this work, but determined based
388 on literature knowledge. For example, triglycerides and proteins are storage for NEFAs and amino
389 acids, respectively. However, while it is commonly assumed that glycogen is the storage for
390 glucose, we recognize literature evidence pointing to other forms of tissue storages for glucose,
391 such as proteins (Shipley et al., 1967, 1970). Furthermore, as glucose is a substrate for the glycerol
392 backbone of tissue TAG, there is likely substantial flux from glucose to this form of nutrient
393 storage. A thorough investigation of the storages with new experimental designs would be a
394 critical future objective. Our work focused on establishing the flux framework and for this
395 purpose only studied fasted male mice. Application of this framework to female animals and to
396 other physiological conditions is of great importance.
397
398 **ACKNOWLEDGEMENTS**
399 The authors thank all current members and alumni of the Hui lab for their assistance and
400 discussion in the research. This research was supported by the Paul G. Allen Family Foundation

401 0034665 (S.H.), the NIH R00DK117066 (S.H.), and the Sabri Ülker Center for Metabolic Research.
402 Some figures were created with BioRender.com.
403
404 **AUTHOR CONTRIBUTIONS**
405 B.Y. designed and conducted the experiment, analyzed data, and wrote the manuscript. K.I.
406 supervised and assisted with the metabolic cage measurement. G.H. co-supervised the metabolic
407 cage measurement and proposed critical revision to the manuscript. S.H. conceived and
408 supervised the project, secured funding, and wrote the manuscript. All authors reviewed and
409 contributed feedback to the manuscript.
410
411 **DECLARATION OF INTERESTS**
412 The authors declare no competing interests.
413
414

415 **STAR METHODS**

416 **KEY RESOURCES TABLE**

REAGENT or RESOURCE	SOURCE	IDENTIFIER
Chemicals, Peptides, and Recombinant Proteins		
D-glucose ($^{14}C_6$)	PerkinElmer	NEC042V250UC
D-glucose ($^{13}C_6$, 99%)	Cambridge Isotope Laboratories	CLM-1396
sodium L-lactate ($^{13}C_3$, 98%) 20% w/w in H_2O	Cambridge Isotope Laboratories	CLM-1579
L-alanine ($^{13}C_3$, 99%)	Cambridge Isotope Laboratories	CLM-2184-H
L-glutamine ($^{13}C_5$, 99%)	Cambridge Isotope Laboratories	CLM-1822-H
glycerol ($^{13}C_3$, 99%)	Cambridge Isotope Laboratories	CLM-1510
sodium D-3-hydroxybutyrate ($^{13}C_4$, 99%)	Cambridge Isotope Laboratories	CLM-3853
sodium acetate ($^{13}C_2$, 99%)	Cambridge Isotope Laboratories	CLM-440
sodium palmitate ($^{13}C_{16}$, 98%)	Cambridge Isotope Laboratories	CLM-6059
oleic acid, potassium salt ($^{13}C_{18}$, 98%)	Cambridge Isotope Laboratories	CLM-8856
linoleic acid, potassium salt ($^{13}C_{18}$, 98%)	Cambridge Isotope Laboratories	CLM-8835
L-valine ($^{13}C_5$, 99%)	Cambridge Isotope Laboratories	CLM-2249-H
bovine serum albumin, fatty acid free, ≥96%	Sigma-Aldrich	A6003
glycerokinase	Sigma-Aldrich	G6278
Experimental Models: Organisms/Strains		
Mouse: C57BL/6J	Jackson laboratory	000664
Mouse: ob/ob <HO>	Jackson laboratory	000632
Software and Algorithms		
El-MAVEN software	Elucidata https://docs.polly.elucidata.io/index.html	
RStudio	Posit https://posit.co/download/rstudio-desktop/	
AccuCor	Github: https://github.com/XiaoyangSu/AccuCor	
Biorender	Biorender https://www.biorender.com/	
Others		
chow diet	PicoLab Mouse Diet 20	5058
high fat diet	Research Diets	D12492i
XBridge BEH Amide XP column	Waters	176002889
Acquity UPLC BEH C18 column	Waters	186003719
catheter for mouse jugular vein	Instech Laboratories	C20PUMJV1301
catheter for mouse carotid artery	Instech Laboratories	C10PU-MCA1459
vascular access button, 1 channel	Instech Laboratories	VABM1B/25
vascular access button, 2 channels	Instech Laboratories	VABM2B/25R25
tether for 1 channel button	Instech Laboratories	VABM1T/25
tether for 2 channel button	Instech Laboratories	VABM2T/25
Buprenorphine base ER 0.5 mg/mL	Wedgewood	Rx # 7270862
Swivel	Instech Laboratories	375/25PS
counter balanced arm	Instech Laboratories	SMCLA
Blood collection Microvette	Starstedt Inc	16.440.100
Heparin sodium 5000 U/mL	McKesson Corp.	-

417

418

419 **RESOURCE AVAILABILITY**

420

421 **Lead Contact**

422 Additional information and requests for resources should be directed to the Lead Contact, Sheng
423 Hui (shui@hsph.harvard.edu).

424

425 **Materials AVAILABILITY**

426 No new reagents were generated in this study.

427

428 **Data and Code Availability**

429 Raw data and R scripts used for flux analysis is available on GitHub
430 (https://github.com/yuanboFaith/flux-model-energy-metabolism).

431

432 **EXPERIMENTAL MODEL AND SUBJECT DETAILS**

433 All mouse work followed protocols approved by the Institutional Animal Care and Use Committee
434 of Harvard Medical Area. The animals were housed on a normal light cycle (7 AM to 7 PM), and
435 were 12-24 weeks old when used in experiment. The wild type C57BL/6J and ob/ob mice were
436 fed with standard chow (PicoLab Mouse Diet 5058). For diet-induced obese mice, C57BL/6J mice
437 were fed with high fat diet (Research Diets D12492i, 60%kcal from fat) starting from the 3 weeks
438 of age for 3-4 months before experiment. For *in vivo* tracer infusion, a jugular vein catheter (JVC)
439 was inserted into the right jugular vein, under aseptic conditions and with anesthesia using
440 isoflurane. The JVC was tunneled subcutaneously to the back of the interscapular area, and
441 connected to a single-channel vascular access button (VAB). For arterial blood collection, in
442 addition to jugular catheterization, a carotid artery catheter (CAC) was implanted into the left
443 carotid artery. Both the JVC and CAC were subcutaneously tunneled to the interscapular region,
444 and connected to a double-channel VAB. The catheter patency was maintained by sealing with
445 lock solution composed of 50% glycerol in saline, with 200 U heparin/mL. After surgery, 50 µL of
446 0.5 mg/mL analgesic buprenorphine SR per 25 g body weight was subcutaneously injected to the
447 right flank. The animal was allowed to recover from surgery for at least five days before use in
448 experiment.

449

450 **METHOD DETAILS**

451

452 **$^{13}CO_2$ Measurement**

453 ^{13}C-labeled tracer compounds were prepared in sterile saline. Fatty acids were complexed with
454 bovine serum albumin in a molar ratio of 6:1. For $^{13}CO_2$ measurements after tracer bolus injection,
455 the mouse was transferred to a new cage without food at 9:00 AM. After 4 hours of fasting, the
456 animal was gently warmed by a heat lamp to dilate the tail vein. Under light isoflurane anesthesia,
457 the mouse was administered with 200 µL ^{13}C-tracer solution via the tail vein. The animal was then
458 immediately transferred to a cage in the metabolic cage system, which was equipped with a
459 stable isotope gas analyzer (Promethion, Sable Systems International, NV). Expired $^{13}CO_2$ and
460 metabolic cage parameters including air flow rate, oxygen, and CO_2 were monitored for another
461 6 hours without food access.

462 $^{13}CO_2$ measurement with tracer infusion required catharized mice and followed the same
463 protocol described in the tracer infusion section below, except that the infusion lasted for 3-4
464 hours, with a reduced tracer concentration. The tracer concentration and infusion rates can be
465 found in **Table S1**. $^{13}CO_2$ data and metabolic cage parameters including air flow rate, oxygen, and
466 CO_2 were continuously collected for the entire period of tracer infusion.

467

468 **Infusion of Isotope Tracers**

469 On the day of tracer infusion, the mouse was transferred to a new cage without food at 9 AM,
470 and fasted for 4 hours before infusion. Right before the start of infusion, the lock solution was
471 drawn and removed from the catheter, and the catheter was flushed with 50 µL saline. The VAB
472 was then connected to the infusion tether, which was in turn connected with a swivel on a
473 counter-balance arm. This allowed the mouse to move freely around in the cage. The infusion
474 started at 2 PM, and lasted for 30 min for fatty acids and 2.5-3 h for all other tracers. The tracer
475 concentration and infusion rates can be found in **Table S1**. At the end of infusion, 40 µL blood
476 was collected by tail snip. For infusion of ^{13}C-lactate, alanine, and glutamine, given their
477 significant labeling difference in the arterial and venous blood (**Table S2**)(Lee et al., 2023), 40 µL
478 arterial blood was sampled from the carotid artery via the pre-implanted catheter, and used for

479 analysis. The blood was collected into a Microvette tube with clotting activator, and was kept on
480 ice during collection. After infusion, the catheter was flushed with 50 µL saline, and then sealed
481 with 10 ~ 20 µL lock solution. The blood was centrifuged at 5,000 ×g for 10 min. 4 µL serum was
482 aliquoted in separate tubes, and stored at -80°C.
483
484 **Serum Sample Preparation for LC-MS Analysis**
485 4 µL serum was mixed with 60 µL -20°C methanol: acetonitrile: water at 40: 40: 20. The sample
486 was vigorously vortexed, and centrifuged at 4°C at 13,000 g for 10 min. 30 µL supernatant was
487 transferred to the HPLC vial from which 5 µL was injected to the LC-MS.
488 Serum glycerol was first enzymatically derivatized into glycerol-3-phosphate before LC-MS
489 analysis. 4 µL serum was mixed with 90 µL freshly made enzyme solution containing 2 U/mL
490 glycerol kinase, 25 mM Tris-HCl (pH 8.0), 50 mM sodium chloride, 10 mM magnesium chloride,
491 and 1.5 mM ATP, and incubated at room temperature for 15 min. The reaction was stopped by
492 the addition of 400 µL methanol. The sample was vortexed, and centrifuged at 16,000 g for 10
493 min. The supernatant was transferred to a new tube, and dried using SpeedVac at 45 °C for 90
494 min. 60 µL of methanol: acetonitrile: water at 40: 40: 20 was added to the residue, vortexed, and
495 centrifuged at 16,000 g for 10 min. 30 µL supernatant was transferred to the HPLC vial, from
496 which 5 µL was injected to the LC-MS.
497
498 **LC-MS Analysis**
499 Chromatographic separation was achieved using XBridge BEH Amide XP Column (2.5 µm, 2.1 mm
500 × 150 mm) with guard column (2.5 µm, 2.1 mm × 5 mm) (Waters, Milford, MA). The mobile phase
501 A was water: acetonitrile 95:5, and mobile phase B was water: acetonitrile 20:80, with both
502 phases containing 10 mM ammonium acetate and 10 mM ammonium hydroxide. The elution
503 linear gradient was: 0 ~ 3 min, 100% B; 3.2 ~ 6.2 min, 90% B; 6.5. ~ 10.5 min, 80% B; 10.7 ~ 13.5
504 min, 70% B; 13.7 ~ 16 min, 45% B; and 16.5 ~ 22 min, 100% B, with flow rate of 0.3 mL/min. The
505 autosampler was at 4˚C. The injection volume was 5 µL. Needle wash was applied between
506 samples using methanol: acetonitrile: water at 40: 40: 20. The mass spectrometer used was Q
507 Exactive HF (Thermo Fisher Scientific, San Jose, CA), and scanned from 70 to 1000 *m/z* with

508 switching polarity. The resolution was 120,000. Metabolites were identified based on accurate
509 mass and retention time using an in-house library. ^{13}C-Natural abundance correction was
510 performed in R using package AccuCor (Su et al., 2017).
511
512 **^{14}C-glucose administration and carcass analysis**
513 The mouse was fasted from 9 AM to 12 PM, and then 12 nCi $^{14}C_6$-glucose in 200 µL saline was
514 administered via the tail vein. After 6 h, the animal was sacrificed, and the hair was shaved off.
515 The carcass was transferred into an Erlenmeyer flask containing 70 mL 1.7 M KOH, and
516 microwaved to simmer. The flask was incubated at 90 C° for 3 h for complete carcass digestion.
517 After having cooled down to room temperature, the total liquid volume was measured, and 2 mL
518 15% antifoam B emulsion (Sigma A5757) and 1 mL Tween 80 (Sigma P4780) was added to the
519 digest. Under magnetic stirring, 0.4 mL of the digest was sampled and transferred to a scintillation
520 vial. A mix of 150 µL 2 M acetic acid, 200 µL 50% H_2O_2, and 50 µL 15% antifoam B was added to
521 the vial, followed by incubation at 70C° for 20 min to decolorize the mixture. The vial was then
522 added with 200 µL of 12 M acetic acid and 5 mL Ecolume scintillation liquid (MP Biomedicals,
523 0188247001) and vigorously vortexed. ^{14}C radioactivity in the vial was measured using a HIDEX
524 300 SL liquid scintillation counter (Turku, Finland).
525
526 **QUANTIFICATION AND STATISTICAL ANALYSIS**
527 **Calculation of the Fraction of Oxidation (f_{ox}) of a Circulating Nutrient**
528 The f_{ox} of a circulating nutrient was calculated as the fraction of ^{13}C atoms in the exhaled CO_2
529 among the total ^{13}C atoms in the administered tracer. For a mouse in a metabolic cage system
530 administered with a ^{13}C tracer, the production flux of tracer-derived $^{13}CO_2$ from the animal J
531 (µmol/min) was calculated as

$$J = \frac{Q}{22.4(1 - E_{NA})} \cdot [\, C_{out}(E_{out} - E_{NA}) - C_{in}(E_{in} - E_{NA})] \cdot 10^{-3} \qquad \text{(Equation 8)}$$

532 where Q is the air flow rate through the cage, C_{in} and C_{out} are the CO_2 concentration measured
533 in the air inflow and outflow respectively, E_{in} and E_{out} are the $^{13}CO_2$ enrichment measured in
534 the air inflow and outflow, respectively, and E_{NA} is the ^{13}C natural abundance of the unlabeled

535 nutrients in the mouse body. E_{NA} was calculated using Eq. (8) from measured CO_2 concentration
536 and enrichment data for a non-infused control mouse group and a production flux of tracer-
537 derived $^{13}CO_2$ as zero ($J = 0$). For an animal under the infusion at the rate of R (μmol ^{13}C-
538 atoms/min), the f_{ox} was then calculated as

$$f_{ox} = \frac{J}{R} \qquad \text{(Equation 9)}$$

539 For animal receiving the tracer as a single bolus at dosage of B (μmol ^{13}C-atoms), the fraction of
540 oxidation f_{ox} was calculated as

$$f_{ox} = \frac{1}{B}\int_{t=0}^{\infty} J\, dt \qquad \text{(Equation 10)}$$

541 with integration from the time of injection to the end of measurement when CO_2 enrichment
542 reached basal level. Details of the derivations are in **Suppl. Note 1**.

543

544 **Calculation of Fluxes to Oxidation (J_{OX}) and Storages (J_S) from a Circulating Nutrient**

545 The J_{ox} and J_S were calculated using Eqs. (1) and (2) in the main text, respectively. The labeling
546 L used here and throughout the text was the carbon-atom labeling fraction of the nutrient. It is
547 calculated as

$$L = \frac{1}{N}\sum_{i=1}^{N} i \cdot L_{M+i} \qquad \text{(Equation 11)}$$

548 where N is the number of carbon atoms in a molecule, and L_{M+i} is the fraction of isotopologue
549 containing i number of ^{13}C atoms among all isotopologues of the molecule. Details of the
550 derivations are in **Suppl. Note 2**.

551

552 **Calculation of the *Direct* Fluxes to Oxidation (O) and Storage (S) from Circulating Nutrients**

553 The direct oxidation fluxes O_i of N circulating nutrients were calculated with Eq. (5) in the main
554 text. The direct storing fluxes S_i of the circulating nutrients were calculated with

$$\boldsymbol{A} \cdot \begin{bmatrix} S_1 \\ S_2 \\ \vdots \\ S_N \end{bmatrix} = \begin{bmatrix} R_1(1 - f_{ox_1}) \\ R_2(1 - f_{ox_2}) \\ \vdots \\ R_N(1 - f_{ox_N}) \end{bmatrix} \qquad \text{(Equation 12)}$$

where R_i and f_{ox_i} are the infusion rate and the fraction of oxidation of nutrient i, respectively. The matrix $\boldsymbol{A}$ is defined as

$$\boldsymbol{A} = \begin{bmatrix} \frac{L_1^1}{1 - L_1^1} & \frac{L_2^1}{1 - L_2^1} & \cdots & \frac{L_N^1}{1 - L_N^1} \\ \frac{L_1^2}{1 - L_1^2} & \frac{L_2^2}{1 - L_2^2} & \cdots & \frac{L_N^2}{1 - L_N^2} \\ \vdots & \vdots & \ddots & \vdots \\ \frac{L_1^N}{1 - L_1^N} & \frac{L_2^N}{1 - L_2^N} & \cdots & \frac{L_N^N}{1 - L_N^N} \end{bmatrix} \qquad \text{(Equation 13)}$$

where L_i^j is the labeling of nutrient i under the infusion of ^{13}C-labeled nutrient j. The unknowns O_i and S_i were solved with the method of least squares, subjected to $O_i \geq 0$ and $S_i \geq 0$, using R package LimSolve, and function lsei (least squares with equalities and inequalities) (Soetaert, 2009). The error was approximated with Monte Carlo simulation. For Eqs. (5) and (12), respectively, we ran the matrix optimization 100 times. In each optimization, for each L_i^j and f_{ox_i} value, a random value was drawn from a normal distribution, with mean and standard deviation (SD) being the mean and standard error of the mean (SEM) of these measured quantities. The SD of the 100 simulated $\boldsymbol{O}$ and $\boldsymbol{S}$ vectors were taken as the associated SEM, respectively. More details of the calculation can be found in **Suppl. Note 3**.

Calculation of the Storage Releasing Flux ($\boldsymbol{F_s}$) to a Circulating Nutrient, and Conversion Fluxes ($\boldsymbol{F_i}$) between Circulating Nutrients

To calculate the storage-releasing flux F_s and the converting fluxes F_i from n different circulating nutrients to a target nutrient (TN) of interest, ^{13}C-labeled TN and the n source nutrients were infused individually to the animals. Each infusion generates an Eq. (7), with L_{TN} in replace of L_{glu}. Integrating all $n + 1$ equations gives the linear system

$$\boldsymbol{B} \cdot \begin{bmatrix} F_1 \\ F_2 \\ \vdots \\ F_n \\ F_s \end{bmatrix} = \begin{bmatrix} R(1 - L_{TN}) \\ 0 \\ \vdots \\ 0 \\ 0 \end{bmatrix} \qquad \text{(Equation 14)}$$

with

$$\boldsymbol{B} = \begin{bmatrix} \frac{L_*^* - L_1^*}{1 - L_1^*} & \frac{L_*^* - L_2^*}{1 - L_2^*} & \cdots & \frac{L_*^* - L_n^*}{1 - L_n^*} & \frac{L_*^* - L_s^*}{1 - L_s^*} \\ \frac{L_*^1 - L_1^1}{1 - L_1^1} & \frac{L_*^1 - L_2^1}{1 - L_2^1} & \cdots & \frac{L_*^1 - L_n^1}{1 - L_n^1} & \frac{L_*^1 - L_s^1}{1 - L_s^1} \\ \vdots & \vdots & \ddots & \vdots & \vdots \\ \frac{L_*^n - L_1^n}{1 - L_1^n} & \frac{L_*^n - L_2^n}{1 - L_2^n} & \cdots & \frac{L_*^n - L_n^n}{1 - L_n^n} & \frac{L_*^n - L_s^n}{1 - L_s^n} \end{bmatrix} \qquad \text{(Equation 15)}$$

where $L_s^j = 0$. Asterisks are used in replace of *TN* for notation clarity. The matrix optimization and error estimation were performed as above. More details of the calculation can be found in **Suppl. Note 4**.

Estimation of Energy Wasted in Futile Cycles

The ATP flux that is wasted in the major futile cycles was estimated using the following parameters: a4 ATP molecules wasted per cycling of one glucose molecule in the Cori cycle, 9-11 ATP molecules used in the resynthesis of each TAG molecule in the TAG-NEFA cycling, and 4 ATP molecules used for synthesis of each peptide bond (Bender, 2012). The total flux of ATP generation was calculated based on the direct carbon oxidation flux of circulating nutrients, where the ATP yield is 5.3 per carbohydrate carbon, 6.5 per fatty acid carbon, 5.5 per ketone body carbon, and 5 per amino acid carbon (Bender, 2012). More details of the calculation are in **Suppl. Note 6**.

589 **REFERENCES**

590 Bender, D.A. (2012). The metabolism of “surplus” amino acids. Br. J. Nutr. *108*, 7–10.
591 https://doi.org/10.1017/S0007114512002292.

592 Brownstein, A.J., Veliova, M., Acin-Perez, R., Liesa, M., and Shirihai, O.S. (2022). ATP-consuming futile cycles
593 as energy dissipating mechanisms to counteract obesity. Rev. Endocr. Metab. Disord. *23*, 121–131.
594 https://doi.org/10.1007/s11154-021-09690-w.

595 Coppack, S.W., Persson, M., Judd, R.L., and Miles, J.M. (1999). Glycerol and nonesterified fatty acid
596 metabolism in human muscle and adipose tissue in vivo. Am. J. Physiol. - Endocrinol. Metab. *276*, 233–240.
597 https://doi.org/10.1152/ajpendo.1999.276.2.e233.

598 Elia, M., Fuller, N.J., and Murgatroyd, P.R. (1992). Measurement of bicarbonate turnover in humans:
599 Applicability to estimation of energy expenditure. Am. J. Physiol. - Endocrinol. Metab. *263*.
600 https://doi.org/10.1152/ajpendo.1992.263.4.e676.

601 Fearon, K.C.H., Hansell, D.T., Preston, T., Plumb, J.A., Davies, J., Shapiro, D., Shenkin, A., Calman, K.C., and
602 Burns, H.J.G. (1988). Influence of Whole Body Protein Turnover Rate on Resting Energy Expenditure in Patients with
603 Cancer. Cancer Res. *48*, 2590–2595. .

604 Gorissen, S.H.M., and Phillips, S.M. (2018). Branched-chain amino acids (leucine, isoleucine, and valine) and
605 skeletal muscle (Elsevier Inc.).

606 Hanson, R.W., Ballard, F.J., and Reshef, L. (2006). Glyceroneogenesis, the pathway that almost wasn’t.
607 Biochem. Mol. Biol. Educ. *34*, 317–323. https://doi.org/10.1002/bmb.2006.494034052637.

608 Hinkle, P.C. (2005). P/O ratios of mitochondrial oxidative phosphorylation. Biochim. Biophys. Acta - Bioenerg.
609 *1706*, 1–11. https://doi.org/10.1016/j.bbabio.2004.09.004.

610 Hui, S., Ghergurovich, J.M., Morscher, R.J., Jang, C., Teng, X., Lu, W., Esparza, L.A., Reya, T., Zhan, L., Yanxiang
611 Guo, J., et al. (2017). Glucose feeds the TCA cycle via circulating lactate. Nature *551*, 115–118.
612 https://doi.org/10.1038/nature24057.

613 Hui, S., Cowan, A.J., Zeng, X., Yang, L., TeSlaa, T., Li, X., Bartman, C., Zhang, Z., Jang, C., Wang, L., et al. (2020).
614 Quantitative Fluxomics of Circulating Metabolites. Cell Metab. *32*, 676-688.e4.
615 https://doi.org/10.1016/j.cmet.2020.07.013.

616 Keller, U., Sonnenberg, G.E., and Stauffacher, W. (1981). Validation of a tracer technique to determine
617 nonsteady-state ketone body turnover rates in man. Am. J. Physiol. - Endocrinol. Metab. *3*.
618 https://doi.org/10.1152/ajpendo.1981.240.3.e253.

619 Kleberg, K., Nielsen, L.L., Stuhr-Hansen, N., Nielsen, J., and Hansen, H.S. (2014). Evaluation of the immediate

620 vascular stability of lipoprotein lipase-generated 2-monoacylglycerol in mice. BioFactors *40*, 596–602.
621 https://doi.org/10.1002/biof.1189.

622 Lee, W.D., Liang, L., AbuSalim, J., Jankowski, C.S.R., Samarah, L.Z., Neinast, M.D., and Rabinowitz, J.D. (2023).
623 Impact of acute stress on murine metabolomics and metabolic flux. Proc. Natl. Acad. Sci. *120*, 2017.
624 https://doi.org/10.1073/pnas.2301215120.

625 Liss, K.H.H., Lutkewitte, A.J., Pietka, T., Finck, B.N., Franczyk, M., Yoshino, J., Klein, S., and Hall, A.M. (2018).
626 Metabolic importance of adipose tissue monoacylglycerol acyltransferase 1 in mice and humans. J. Lipid Res. *59*,
627 1630–1639. https://doi.org/10.1194/jlr.M084947.

628 Matthews, D.E., Motil, K.J., and Rorhrbaugh, D.K. (1980). Measurement of leucine metabolism in man from a
629 primed, continuous infusion of L-[1-13C]leucine. Am. J. Physiol. - Endocrinol. Metab. *1*.
630 https://doi.org/10.1152/ajpendo.1980.238.5.e473.

631 Mugabo, Y., Zhao, S., Seifried, A., Gezzar, S., Al-Mass, A., Zhang, D., Lamontagne, J., Attane, C., Poursharifi, P.,
632 Iglesias, J., et al. (2016). Identification of a mammalian glycerol-3-phosphate phosphatase: Role in metabolism and
633 signaling in pancreatic β-cells and hepatocytes. Proc. Natl. Acad. Sci. U. S. A. *113*, E430–E439.
634 https://doi.org/10.1073/pnas.1514375113.

635 Newsholme, E.A. (1978). Substrate cycles: their metabolic, energetic and thermic consequences in man.
636 Biochem. Soc. Symp. 183–205. .

637 Nye, C., Kim, J., Kalhan, S.C., and Hanson, R.W. (2008). Reassessing triglyceride synthesis in adipose tissue.
638 Trends Endocrinol. Metab. *19*, 356–361. https://doi.org/10.1016/j.tem.2008.08.003.

639 Oeckl, J., Janovska, P., Adamcova, K., Bardova, K., Brunner, S., Dieckmann, S., Ecker, J., Fromme, T., Funda, J.,
640 Gantert, T., et al. (2022). Loss of UCP1 function augments recruitment of futile lipid cycling for thermogenesis in
641 murine brown fat. Mol. Metab. *61*, 101499. https://doi.org/10.1016/j.molmet.2022.101499.

642 Possik, E., Klein, L.L., Sanjab, P., Zhu, R., Côté, L., Bai, Y., Zhang, D., Sun, H., Al-Mass, A., Oppong, A., et al.
643 (2023). Glycerol 3-phosphate phosphatase/PGPH-2 counters metabolic stress and promotes healthy aging via a
644 glycogen sensing-AMPK-HLH-30-autophagy axis in C. elegans. Nat. Commun. *14*. https://doi.org/10.1038/s41467-
645 023-40857-y.

646 Reshef, L., Olswang, Y., Cassuto, H., Blum, B., Croniger, C.M., Kalhan, S.C., Tilghman, S.M., and Hanson, R.W.
647 (2003). Glyceroneogenesis and the triglyceride/fatty acid cycle. J. Biol. Chem. *278*, 30413–30416.
648 https://doi.org/10.1074/jbc.R300017200.

649 Scow, R.O., and Blanchette-Mackie, E.J. (1991). Transport of fatty acids and monoacylglycerols in white and
650 brown adipose tissues. Brain Res. Bull. *27*, 487–491. https://doi.org/10.1016/0361-9230(91)90147-C.

651 She, P., Reid, T.M., Bronson, S.K., Vary, T.C., Hajnal, A., Lynch, C.J., and Hutson, S.M. (2007). Disruption of

652 BCATm in Mice Leads to Increased Energy Expenditure Associated with the Activation of a Futile Protein Turnover
653 Cycle. Cell Metab. *6*, 181–194. https://doi.org/10.1016/j.cmet.2007.08.003.

654 Shi, Y., and Cheng, D. (2009). Beyond triglyceride synthesis: The dynamic functional roles of MGAT and DGAT
655 enzymes in energy metabolism. Am. J. Physiol. - Endocrinol. Metab. *297*, 10–18.
656 https://doi.org/10.1152/ajpendo.90949.2008.

657 Shipley, R.A., Chudzik, E.B., Gibbons, A.P., Jongedyk, K., and Brummond, D.O. (1967). Rate of glucose
658 transformation in the rat by whole-body analysis after blucose-14-C. Am. J. Physiol. *213*, 1149–1158.
659 https://doi.org/10.1152/ajplegacy.1967.213.5.1149.

660 Shipley, R.A., Chudzik, E.B., and Gibbons, A.P. (1970). Rate of disposal of glucose carbon to CO2, fat, protein,
661 and glycogen in the diabetic rat. Am. J. Physiol. *219*, 364–373. https://doi.org/10.1152/ajplegacy.1970.219.2.364.

662 Soetaert, K. (2009). Package limSolve, solving linear inverse models in R.

663 Su, X., Lu, W., and Rabinowitz, J.D. (2017). Metabolite Spectral Accuracy on Orbitraps. Anal. Chem *89*, 11.
664 https://doi.org/10.1021/acs.analchem.7b00396.

665 TeSlaa, T., Bartman, C.R., Jankowski, C.S.R., Zhang, Z., Xu, X., Xing, X., Wang, L., Lu, W., Hui, S., and Rabinowitz,
666 J.D. (2021). The Source of Glycolytic Intermediates in Mammalian Tissues. Cell Metab. *33*, 367-378.e5.
667 https://doi.org/10.1016/j.cmet.2020.12.020.

668 Tolbert, B.M., Kirk, M., and Baker, E.M. (1956). Continuous 14CO2 and CO2 Excretion Studies in Experimental
669 Animals. Am. J. Physiol. Content *185*, 269–274. https://doi.org/10.1152/ajplegacy.1956.185.2.269.

670 Wang, Y., Kwon, H., Su, X., and Wondisford, F.E. (2020). Glycerol not lactate is the major net carbon source
671 for gluconeogenesis in mice during both short and prolonged fasting. Mol. Metab. *31*, 36–44.
672 https://doi.org/10.1016/j.molmet.2019.11.005.

673 Wolfe, R.R., Herndon, D.N., Jahoor, F., Miyoshi, H., and Wolfe, M. (1987). Effect of Severe Burn Injury on
674 Substrate Cycling by Glucose and Fatty Acids. N. Engl. J. Med. *317*, 403–408.
675 https://doi.org/10.1056/NEJM198708133170702.

676

677

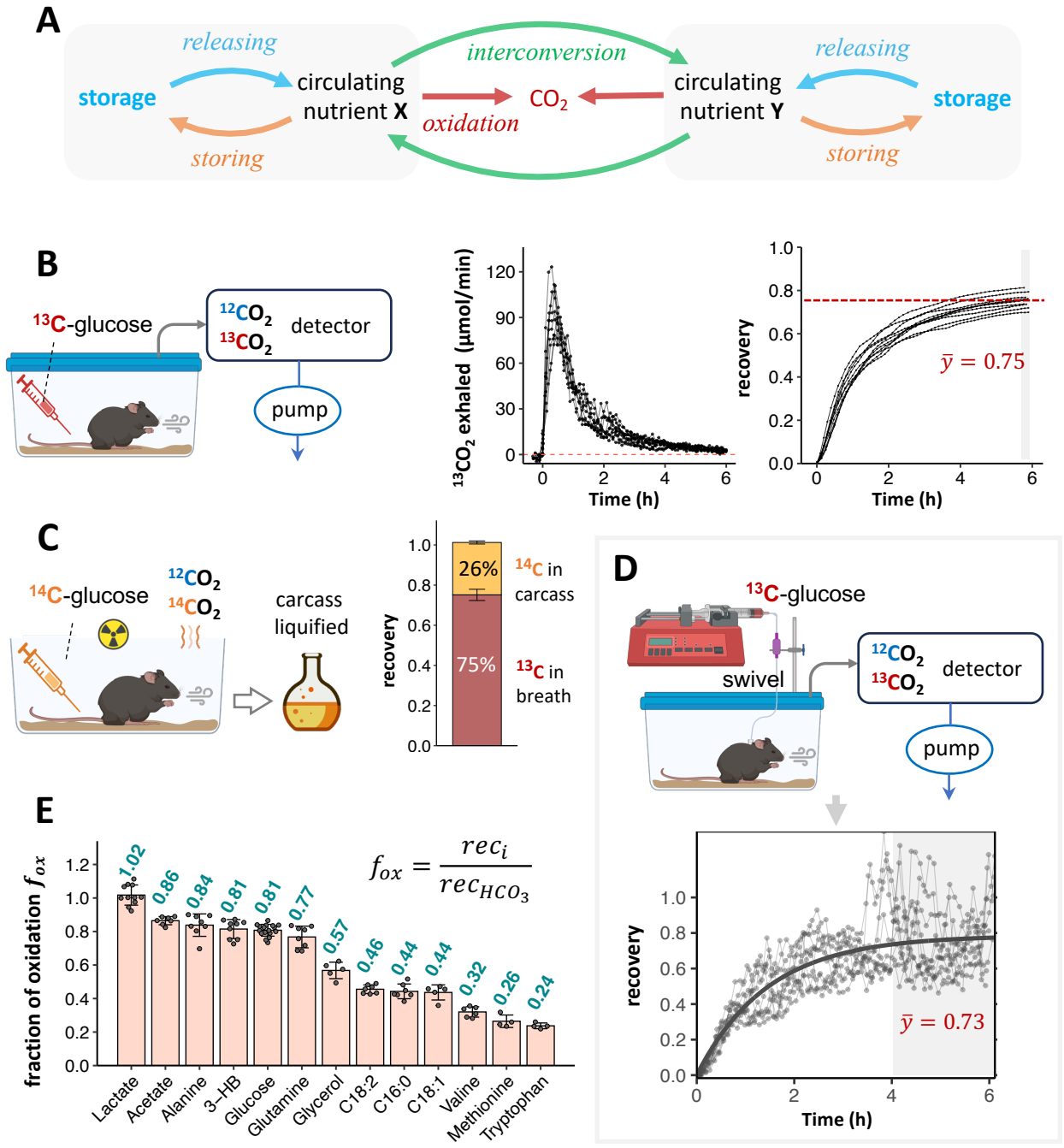

Figure 1. $^{13}CO_2$ Tracing Unveils Characteristic Oxidation and Storing Partition of Circulating Nutrients.

(A) Schematic of the releasing, storing, oxidation, and interconversion of circulating nutrients.

(B) Tracing of $^{13}CO_2$ production after intravenous (i.v.) injection of a nonperturbative bolus dose of ^{13}C-glucose. The $^{13}CO_2$ production kinetics (middle) and accumulated ^{13}C recovery (right)

are shown. Each line represents data from one animal. n = 10.

(C) Deposit of ^{14}C radioactivity in the carcass 6h later after i.v. injection of ^{14}C-glucose. n=3.

(D) Tracing of $^{13}CO_2$ production using nonperturbative i.v. infusion of ^{13}C-glucose in conscious unrestrained animal. Shown are the experimental setup (top) and ^{13}C recovery (bottom). Each thin line represents data from one animal and the thick line is fitted with formula $\mathrm{y} = \mathrm{a} \cdot (1 - \mathrm{e}^{-\mathrm{b} \cdot \mathrm{t}})$. n = 10.

(E) Values of fraction of oxidation (f_{ox}) of 13 major circulating nutrients. Mean ± SD. n = 4 to 17 for individual nutrient, as noted in the scatterplot.

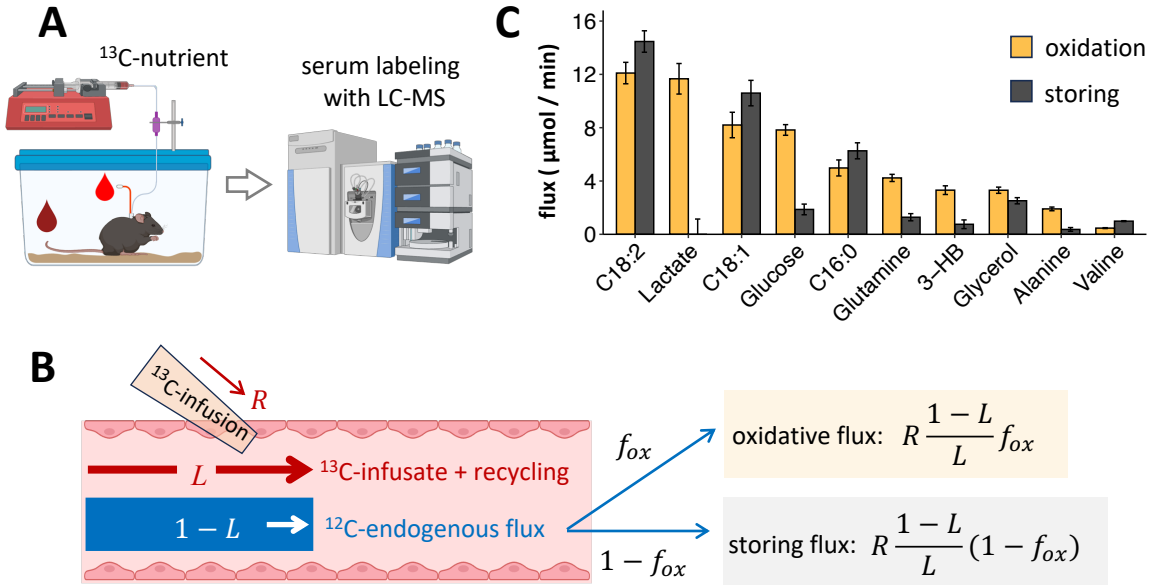

692

693 **Figure 2. Quantification of the Oxidation and Storing Fluxes of Circulating Nutrients.**

694 **(A)** Schematic showing infusion of ^{13}C-nutrient to mice and analysis of the serum labeling with

695 LC-MS. Blood was collected from arterial blood via pre-implanted catheter and/or by tail snip.

696 **(B)** Illustration of the formula for calculating oxidation and storing fluxes of circulating

697 nutrients. R, infusion rate of ^{13}C-nutrient; L, serum labeling of the infusate; and f_{ox}, fraction of

698 oxidation, quantified in Figure 1.

699 **(C)** Oxidation and storing fluxes of major circulating nutrients. Mean ± SEM. For individual

700 nutrient, for their labeling in serum, n = 4~15 (see Figure S3A); for f_{ox}, n = 4 to 17 (Figure 1E); the

701 same replication applies to all figures computed from these two sets of parameters in Figures 2-

702 5 and related supporting figures.

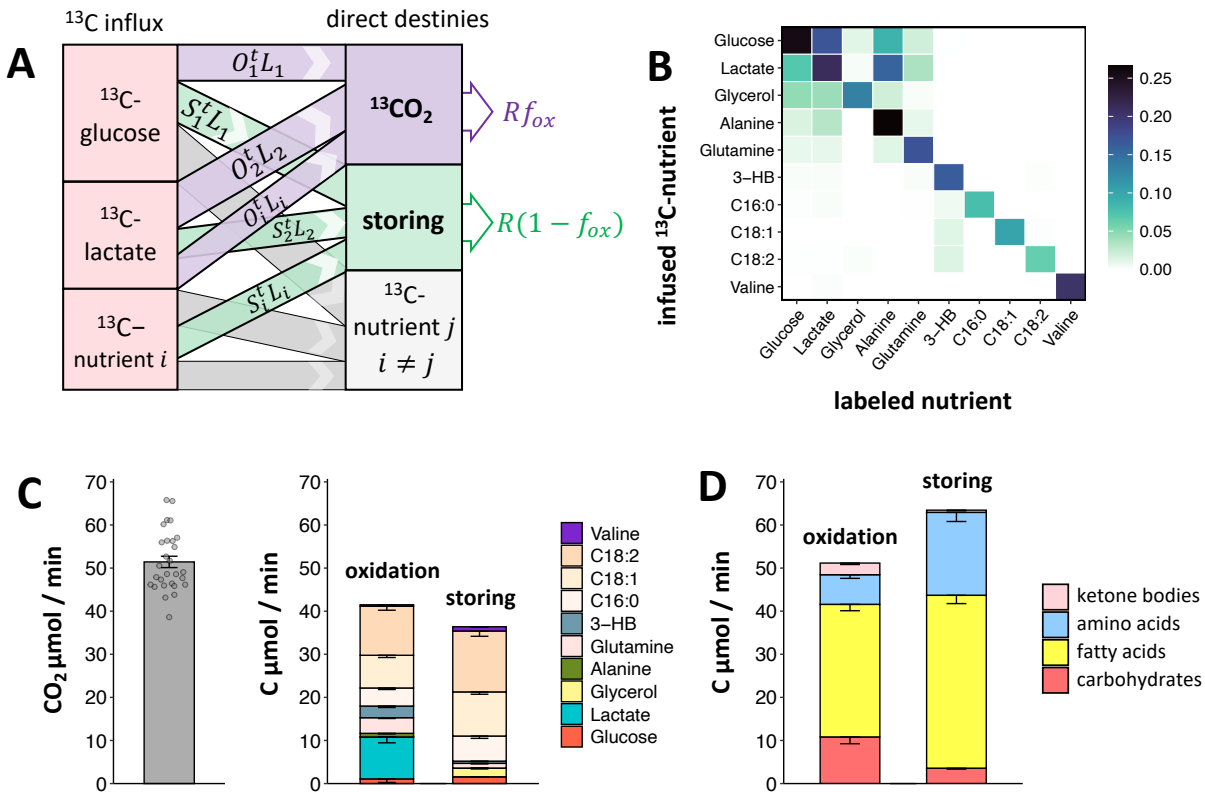

Figure 3. Quantification of *Direct* Oxidation and Storing Fluxes of Circulating Nutrients.

(A) Illustration for calculating direct oxidation and storing fluxes of circulating glucose. At the isotopic steady state of ^{13}C-glucose infusion, the total $^{13}CO_2$ production (oxidation) and storing flux of the ^{13}C-infusate are depicted as the sum of the direct oxidation and storing fluxes from all labeled circulating nutrients, respectively. O_i^t, S_i^t, and L_i are respectively the oxidation flux, storing flux (superscript t for total, including both ^{12}C and ^{13}C), and ^{13}C labeling of circulating nutrient i; R, infusion rate of ^{13}C-glucose; f_{ox}, fraction of oxidation of glucose.

(B) Labeling of circulating nutrients under the infusion of different ^{13}C-nutrients. n = 4 to 15 for individual nutrient (see Figure S3A).

(C) Total CO_2 production (left, n = 28), in comparison with the direct oxidation and storing fluxes of the major circulating nutrients covered in this study (right).

(D) Direct oxidation and storing fluxes of all major circulating nutrients, including carbohydrates (glucose, lactate, and glycerol), fatty acids, protein-originated amino acids, and ketone bodies.

All data is presented in mean ± SEM.

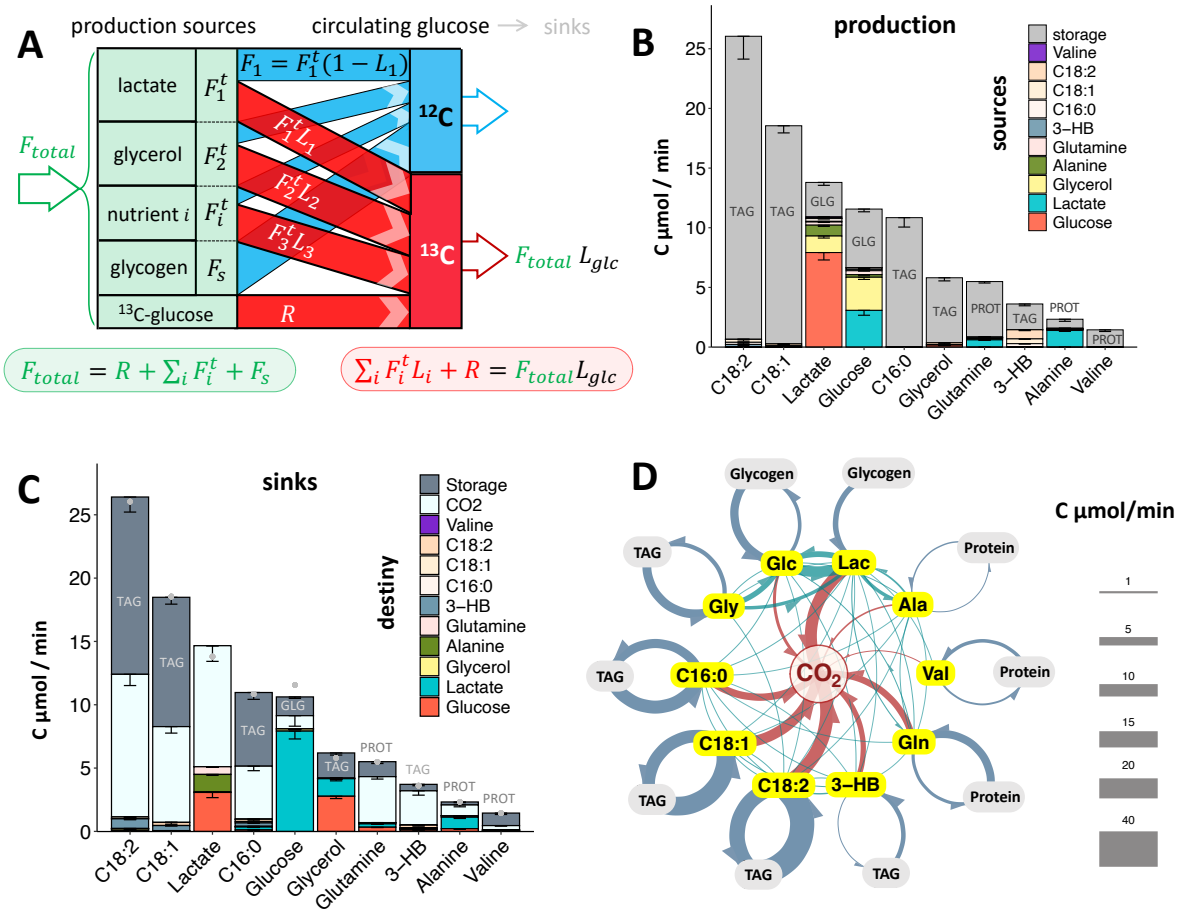

Figure 4. Quantifying Storage Releasing Flux and Interconverting Fluxes for Circulating Nutrients, and Integrating them with Oxidation and Storing Fluxes into a Holistic Flux Model of Circulating Nutrients.

(A) Illustration for calculating the storage releasing flux (glycogenolysis) and gluconeogenic fluxes to produce circulating glucose. R, the ^{13}C-glcose infusion rate; L_{glc}, the labeling of glucose; L_i, the labeling of nutrient i; F_i^t, the production flux from nutrient i to glucose, superscript t for total (including both ^{12}C and ^{13}C); F_s, the releasing flux from storage of glycogen.

(B) The production fluxes of circulating nutrients from storage and other circulating nutrients. TAG, triglyceride; GLG, glycogen, PROT, protein.

(C) Sink fluxes of circulating nutrients, fated to oxidation, storage, and other circulating nutrients. The dot shows the total production flux as quantified in Figure 4B.

(D) An organism-level metabolic map of circulating nutrients. All flux arrows are drawn in counter-clockwise direction. All data is presented in mean ± SEM

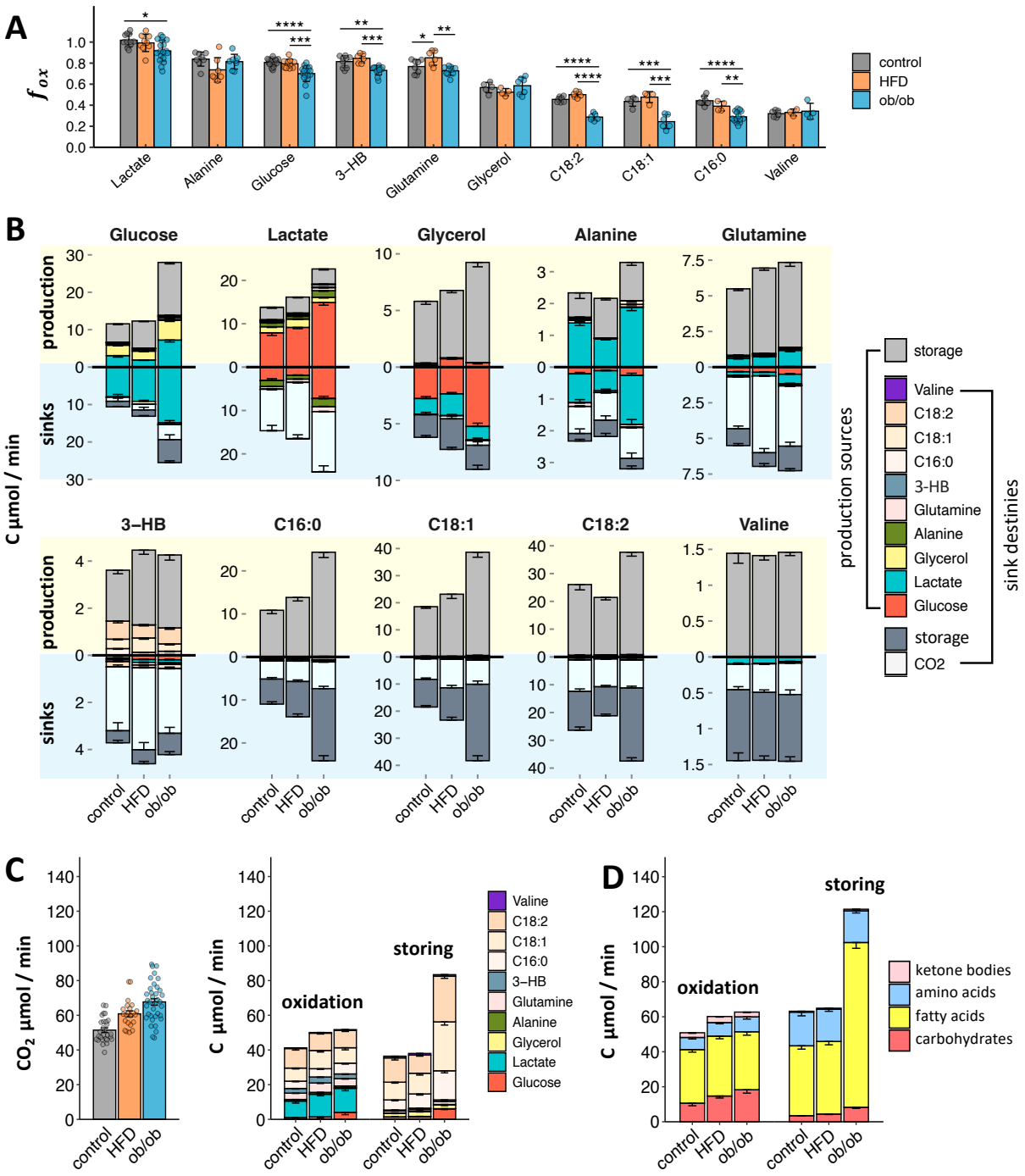

Figure 5. Systematic Flux analysis of Circulating Nutrients in High Fat Diet- Fed (HFD) and ob/ob Mice

(A) Fraction of oxidation (f_{ox}) of circulating nutrients in chow-fed wild type control mice, and the obese mice. Mean ± SD.

(B) Production and sink fluxes of circulating nutrients in the control and obese mice.

739 **(C)** Total CO_2 production (left), and the direct oxidation and storing fluxes of circulating
740 nutrients (right) in the control and obese mice.
741 **(D)** Direct oxidation and storing fluxes of all major circulating nutrients, including
742 carbohydrates (glucose, lactate, and glycerol), fatty acids, protein-originated amino acids, and
743 ketone bodies.
744 **(E)** All data presented in mean ± SEM unless otherwise specified. *p < 0.05, **p < 0.01,
745 ***p<0.001, ****p<0.0001 by Student's *t* test after Bonferroni adjustment. Regarding individual
746 nutrient and phenotype, for f_{ox}, n = 3 to 19 (see scatterplot in panel A); their labeling in serum,
747 n = 4 to 27 (see Figure S6). The same replication also applies to the related supporting figures.
748

749

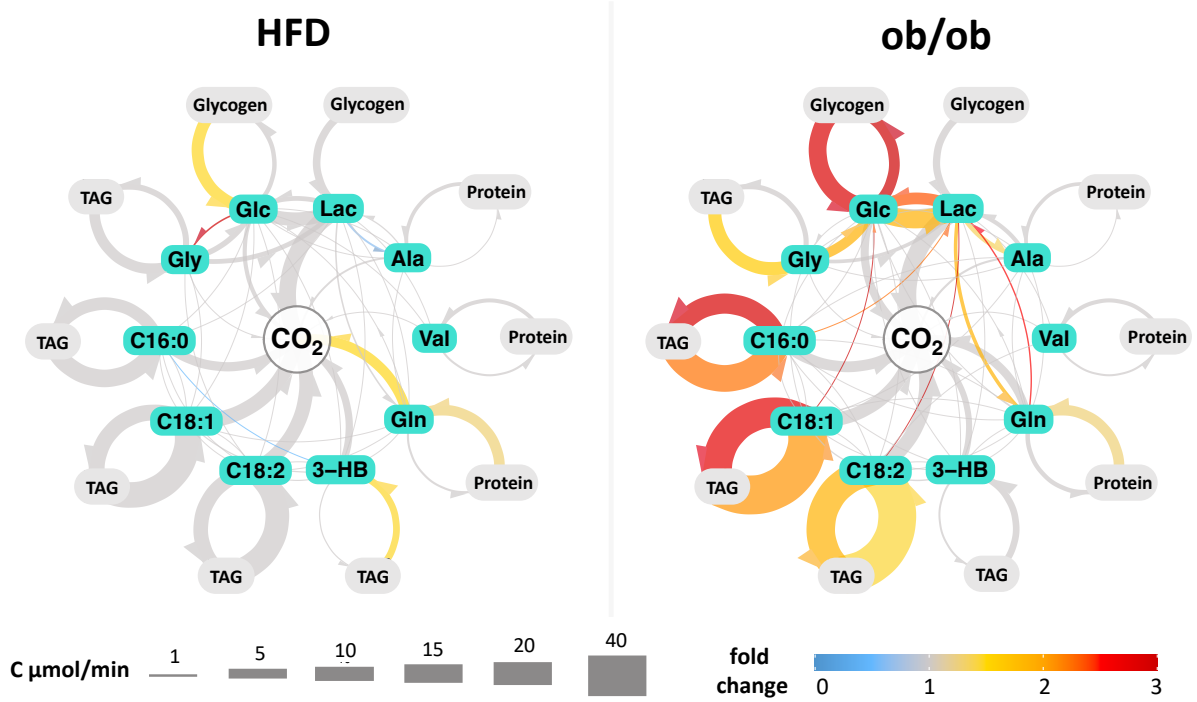

750

751 **Figure 6. Flux Models of Obese Mice Reveals Elevated Metabolic Cycling in ob/ob Mice, but Not**

752 **in High Fat Diet-Fed Mice.**

753 Fluxes in obese mice that are statistically significant (Bonferroni-adjusted p value < 0.05) from

754 the control mice are highlighted in color, with fold change mapped to the color scale. All flux

755 arrows are drawn in counter-clockwise direction.

756